HHS Public Access

Author manuscript

ACS Appl Mater Interfaces. Author manuscript; available in PMC 2017 June 30.

Published in final edited form as:

ACS Appl Mater Interfaces. 2017 March 01; 9(8): 7399–7405. doi:10.1021/acsami.6b13954.

Drug-Derived Bright and Color-Tunable N-doped Carbon Dots for Cell Imaging and Sensitive Detection of Fe^{3+} in Living Cells

Yang Song[1], **Chengzhou Zhu**[1], **Junhua Song**[1], **He Li**[1], **Dan Du**[1,2,*], and **Yuehe Lin**[1,*]

[1]School of Mechanical and Materials Engineering, Washington State University, Pullman, WA 99164

[2]Key Laboratory of Pesticides and Chemical Biology, Ministry of Education, College of Chemistry, Central China Normal University, Wuhan, 430079, PR China

Abstract

Chemical heteroatom doping of carbon dots (CDs) provides effective progress of physicochemical as well as photochemicl properties of CDs. Inspired by the diverse drug compounds with various heteroatoms (such as N, S, P) in the drug library, facile synthesis of a new kind of bright and color tunable N-doped carbon dots (NCDs) has been reported by using a popular antibiotic—aminosalicylic acid as precursor. The N doping of CDs enable effective advaced progress of photoluminescence (PL) efficiency and tunability of PL emission, but also enrichs surface functional groups to broaden its application. The as-prepared NCDs possess tunable PL and shows a quantum yield of 16.4%, which is the result of PL improvement effect of introduced nitrogen atoms among CDs. The cellular toxicity on H1299 cancer cells indicates that the NCDs have properties of negligible cytotoxicity, excellent biocompatibility, and great resistance to photobleaching. Moreover, the drug derived NCDs showed excellent sensitivity in detection of Fe^{3+} in living cells, which indicates the potential application in diagnosis and related biological study.

TOC image

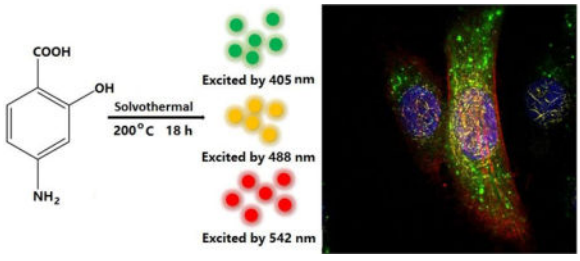

*Corresponding Authors: yuehe.lin@wsu.edu; dan.du@mail.ccnu.edu.cn.

Supporting Information

The Supporting Information is available free of charge on the ACS Publication website at ^{1}H-NMR spectra, High-resolution XPS spectra, Quantum yield, Dynamic Light Scattering, stability and cellular cytotoxicity of NCDs.

Notes

The authors declare no competing financial interest.

Keywords

carbon nanodots; nitrogen doping; color tuning; cell imaging; Fe^{3+} detection

INTRODUCTION

Fluorescent nanomaterials, such as fluoresence nanoclusters and graphene quantum dots (QDs), have been research hotspots recently.[1–4] QDs have great promise for diverse applications, ranging from bioimaging,[5] biosensing,[6] photocatalysis[7] to optoelectronic devices.[8, 9] However, the toxicity issue of QDs is a big concern. Continuous efforts are being made to develop better fluorescent nanomaterials. Now, carbon dots (CDs) have gained ever-increasing attention with superior merits of high water solubility, good biocompatibility, low cytotoxicity and unique photoluminescence (PL) properties.[6, 10–19] Very recently, CDs have been used for real-time molecular tracking in live cells, which shows some advantages over organic fluorophores and semiconductor QDs[38]. However, there are some bottlenecks for preparing CDs with long-wavelength and multicolor emission properties.[20] Thus, it is still highly urgent to develop novel methods to resolve the challenges.[7, 21–24] Recently, heteroatom doping presented a promising strategy for addressing the issues[39]. It is well known that nitrogen (N) is the popular atom for synthesis of heteroatom-doped CDs due to the similarity of atomic size of N and C and the strong bonding between them. Inspired by the diverse drug compounds with various heteroatoms (such as N, S, P) in the drug library, we proposed an effective method to prepare bright and color tunable N-doped CDs (NCDs) with long wavelength emission from drugs. Herein, we report a facile hydrothermal process to prepare multicolor NCDs (with red, yellow, and green emission) from a popular antibiotic —aminosalicylic acid (ASA). As proof of concept demonstration, the as-prepared NCDs have been used for cell imaging and sensitive detection of Fe^{3+} in living cells.

EXPERIMENTAL SECTION

Chemical and materials

4-Aminosalicylic acid was purchased from Sigma-Aldrich. Hydrochloric acid (HCl, 39%) was of analytical grade and purchased from local suppliers. Fetal bovine serum (FBS) was purchased from ATCC. RPMI-1640 Media were supplied by Gibco Invitrogen. The H1299 and MCF-7 cell line was ordered from ATCC. For cell cultures, collagen G, Eagle's medium, L-glutamine, gentamycin, penicillin and streptomycin were purchased from ATCC. Other reagents related to cell experiments were purified and sterilized. Millipore DI water was used for whole experiments.

Measurements

Transmission electron microscopy (TEM) images were captured by Philips CM200 UT (Field Emission Instruments, USA). UV-vis spectra were recorded by AueaMate 8000 spectrometer. The fluorescence spectra were obtained Cary Eclipse fluorimeter, respectively. The Raman spectrum was recorded on a LABRAM HR800 excited by 532 nm laser. Dynamic Light Scattering (DLS) measurements were measured by Nano ZS equipped with a solid-state He-Ne laser (λ=633 nm). X-ray Diffraction (XRD) characterization was achieved

by Rigaku Miniflex 600. Leica SP8 Point Scanning Confocal laser fluorescence microscope was used for relative cell imaging.

Synthesis of NCDs

Aminosalicylic acid (0.2 g) was first dissolved in 20 mL ethanol and transferred into PTFE autoclaves. After heating at 200 °C for 18 h, dark brown aqueous solution was obtained. The solution was purified with a dialysis bag (MWCO ~ 3.3 KDa) for 1 day to dialysis the non-reactive molecules. The DI water would be replaced every 3 h, and finally NCDs were freeze dried to form black solid. We found NCDs are soluble in aqueous solution and most organic solvents including DMSO, ethanol and DMF.

Determination of quantum yield (QY)

Rhodamine B (ethanol; relative QY ~ 0.56) was chosen as a reference. The QY of NCDs were calculated:

$$\phi=\phi' \times \frac{A'}{I'} \times \frac{I}{A} \times \frac{n^2}{n'^2}$$

where as ϕ is QY of the NCDs, I is the integrated emission intensity of NCDs, n is the solvent refractive index (1.36 for ethanol) and A represent the optical density, respectively. The superscript “,” indicated the reference data. For achieving the precious results, various concentrations of NCDs and referenced samples were adjusted the absorption below 0.10 (fluorescence cuvette). The PL spectra were recorded with the fluorimeter.

Cell Imaging

NCDs solution was freeze dried to form black solid in the vacuum freeze dryer. The resulting NCDs powder was re-dispersed into cell culture medium as stocking medium. The stocking medium (NCDs ~50 μg μL^{-1}) was pulsed to the H1299 cancer cells (total medium ~ 2 mL). After 4 hours incubation at 37°C and 5% of CO_2, the cancer cells were washed with PBS for three times before the cell imaging. For Fe^{3+} detection *in vitro*, the cells were co-cultured with 25 μg μL^{-1} NCDs with 0.1 mM or 0.25 mM Fe^{3+}, respectively. After incubation for 8 h, the cells were washed with cold PBS for the cell imaging.

Cytotoxicity assay

The cytotoxicity of NCDs for H1299 cells *in vitro* was performed by the standard MTT assay. H1299 cells were seeded into the 96-well plate at the density of 1.0×10^5 per mL for 24 hours. Then the cells were removed with DMEM medium containing the NCDs with various concentrations for another 24 hrs. After that, the cells were pulsed with 20 μL of MTT (5 mg mL^{-1} in PBS) for 4 hrs. Then, 150 μL DMSO was injected into each well. Finally, the absorption could be recorded at the wavelength of 490 nm.

RESULTS AND DISCUSSION

3.1. Characterization of NCDs

The preparation of NCDs can be accomplished by heating ASA in ethanol at 200°C for 18 hours and then purifying using tubular dialysis membrane (Figure 1a). The resulted NCDs could be homogeneously dispersed into various solvents. It was shown that NCDs were dispersed in water and phosphate buffer solution (PBS), producing a brown solution and a dark red solution, respectively (Figure 1b). Transmission electron microscopy (TEM) was used to investigate the morphology of asprepared NCDs. As revealed in Figure 1c, NCDs have an average size of about 6 nm with uniform spherical structure. The high-resolution TEM (HRTEM) of NCDs clearly indicated that the as-prepared NCDs have high crystalline structure with well-resolved lattice fringes with the relative interplanar distance around 0.21 nm, corresponding to that of the (001) plane of graphite (Figure 1d).[25] As shown in Figure 2a, the XRD pattern is evident that there is a broad diffraction peak centred at $2\theta = 22°$ with the interlayer spacing of 0.395 nm, which is broader than that of graphite (0.34 nm). The broader interlayer space is attributed to richen surface oxygen groups of NCDs.[26, 27] Moreover, the NCDs were investigated by using ^{1}H NMR spectroscopy. The ^{1}H NMR spectrum shown in Figure S1, indicating the signal regions located at 1–3 ppm (for sp^3 C-H protons), 3–6 ppm (for the protons attached with hydroxyl and carbonyl groups), 6–9 ppm (for the aromatic or sp^2 protons). In addition, Fourier transform infrared (FT-IR) spectra were used to investigate surface functional groups of NCDs. As shown in Figure 2d, the NCDs possessed verities of absorption bands of O-H and N-H stretching vibrations of amine groups (3425 cm^{-1}), C-O (1225 cm^{-1}), C-H bending (1457 cm^{-1}), C-O-C vibrations in esters or epoxy (1072 cm^{-1}), C=C (1512 cm^{-1}) and N-H bending (1627 cm^{-1}), indicating the existence of amino bending and aromatic ring structures. Moreover, absorption bands of carbonyl C=O vibrations was also included in this broad band (~ 1652 cm^{-1}).[40–41] These results indicate the successful doping of N atoms into NCDs. In addition, the resultant CDs with profuse surface hydrophilic groups (hydroxyl, carbonyl, and amino) were endowed with promising PL properties along with good polarity and aqueous dispensability. In addition, the zeta potential of the NCDs was shifting from 8.02 mV (positive charge) to −25.41 mV (negative charge) along with pH increasing from 2 to 11, suggesting the protonation and deprotonation of surface groups (Table S1).

The as-prepared NCDs were also characterized using X-ray photoelectron spectroscopy (XPS). As shown in Figure 2b, full-scan XPS spectra presented distinct peaks locating at 284.0, 398, and 530.6 eV, which are attributed to C1s, N1s, and O1s, respectively. In addition, atomic ratio of C1s, N 1s and O 1s was 74.28%, 8.47% and 16.13%, respectively, indicating that high fraction of N atoms was successfully doped into NCDs. The detailed XPS spectra of C 1s (Figure S2a), N 1s (Figure S2b) and O 1s (Figure S2c) further confirmed the existence of C-C/C=C, C-N, C-O-C, C-O, and N-H bonds in NCDs. The Raman spectrum of NCDs was featured by two obvious peaks: the D band (sp^3-hybridized) at 1350 cm^{-1} and the G band (sp^2-hybridized) at 1590 cm^{-1} (Figure 2c).[28, 29] The intensity ratio of the D- to G- bands (I_D/I_G) is often proportional to defect degree in graphite carbon. The I_D/I_G was 0.83, indicating NCDs contained high degree of defects.

Figure 3a exhibited UV-Vis absorption spectra of the NCDs and ASA. NCDs showed relatively rare broad visible range absorption bands, indicating the existence of some electronic absorption transitions.[30] In UV-Vis absorption spectra (from 200nm to 300 nm, Figure S3), the broad absorption band located at 292 nm corresponding to aromatic **π** system, which is similar to that of polycyclic aromatic hydrocarbons. The expected excitation-dependent multicolor emission feature was obviously observed in Figure 3b. Following the increase of excitation wavelength from 360 nm to 600 nm, the emission wavelength increases from 416 nm to 646 nm, as in case of most of carbon nanodots. The excitation-dependent multicolor emission property may be corresponding to to surface chemical functional groups[10, 31, 32] and surface state.[28, 29, 33] As shown in XPS and FTIR, the synthesized NCDs exhibited abundant functional groups, including C-O, C-O-C, C=O on the surface which resulted in emissive traps between **π** and **π*** state of C=C. These emission traps could dominate the emission of NCDs. In particular, it has been demonstrated that the PL origin of CDs may be from the molecule-like state that contain carboxyl, carbonly and amide-based hybrid surface structures. Both the surface state and functional groups are attributed to the complexity of excited states of NCDs[10, 31]. The quantum yields (QYs) of as-prepared NCDs were measured to be 16.4% and 5.8% with excitation at 365 nm and 510 nm using Rhodamine B as reference, respectively (Figure S4).

3.2. Photostability and Cytotoxicity Study of NCDs

For biomedical applications, the drug derived NCDs should have superior biocompatibility, satisfactory photostability and low cytotoxicity. As shown in Figure S5, NCDs were homogeneously dispersed in water, PBS and cell culture medium without any aggregation. Further dynamic light scatting (DLS) testing indicated that the size distribution of NCDs was almost unchanged even after one week (Figure S6), showing the excellent stability of NCDs. Moreover, PL intensity of NCDs could remain stable at relative high ionic strengths (up to 20 mM PBS) or under broad pH ranges (pH 4–11) (Figure S7a and S7b). Besides, the NCDs exhibit better photostability compared to CdSe/ZnS QDs. As shown in Figure 3d, the PL of CdSe/ZnS QDs is quickly quenched in one hour UV irradiation due to photobleaching, while the fluorescence of NCDs is extremely stable, preserving ~ 86% of the initial intensity after one hour of UV irradiation (Figure 3c). Such remarkable photostability is attributed to the surface structure and composition of NCDs. The cytotoxicity of the NCDs was further investigated by the standard MTT assay. More than 92.8 % cells could survive after incubation with NCDs even at concentrations rising from 1.0 to 75 μg mL^{-1} for 24 h, indicating the negligible cytotoxicity of the NCDs (Figure 4). Since the NCDs have demonstrated good biocompatibility, excellent antiphotobleaching ability as well as low cytotoxicity, NCDs were expected to have great potential for biomedical applications including bioimaging and biosensing.

3.3. Cellular Uptake Measured by Confocal Laser Scanning Microscopy

The high PL stability and low cytotoxicity confirm the suitability of these NCDs for bioimaging applications. Figure 5 shows that after pulsing with 50 μg mL^{-1} of NCDs for 4 h, the confocal laser fluorescence microscope (CLSM) images were achieved with distinct lasers excitation. The CLSM displayed intense green, yellow, and red emissions in H1299 cells (Figure 5) under 405, 488, and 542 nm laser excitation, respectively. Here, the cell

nuclei were stained by DAPI as reference. The merged images revealed that the emission was mainly from the cytoplasmic area, demonstrating that the NCDs exhibit efficient endocytic uptake of cultured H1299 cells and successfully localization into cytoplasm. The NCDs are negatively charged particles when pH around 7, so it is highly unlike that they enter cells by passive processes because of the electrostatic repulsion. It is due to the endocytotic process of NCDs and subsequently trafficked along the endosomal network. The as-prepared NCDs were excluded from the nucleus and concentrated at cytoplasm. For further investigation of endocytotic process of NCDs, the intracellular trafficking images were further evaluated. It was known that some NPs could escape from the endosomes into the cytoplasm by vesicle breakdown after endocytosis. In order to track the NCDs internalized pathway, we labeled H1299 cancer cells with Lyso-Tracker (lysosome stain) and Cytoskeleton-Actin (Actin stain). The cells labeled with NCDs and Lyso-Tracker need to be separately incubated to avoid Förster resonance energy transfer (FRET). The quantitative co-localization analysis of NCDs-labeled structure generally showed a less colocalization with Lyso-Tacker (Pearson's correlation coefficient, ρ=0.227) but higher colocalization with Cytoskeleton-Actin (Pearson's correlation coefficient, ρ=0.54), suggesting that the particles exhibit minimal endolysosomal trapping[34, 35] (Figure 6a). Moreover, the fluorescence microscopy of H1299 cells showed that most of NCDs remained at the cell cytoplasm (Figure 6b), which was evidenced by rare overlap fluoresence signals. The above observation was verified by quantifying fluorescence intensity of the line scanning profiles (Figure 6b). In Figure 6c, the cross-sectional CLSM images for the H1299 cells incubated with the NCDs also verified that particles were located at the regions, a further confirmation of their effective endosome escape. The endosome escape most probably because that the untreated amino group of NCDs could provide high buffering capacity to trigger the osmotic swelling and physical rupture of the lysosomes in acid vesicle (well-known as proton-sponge).[36, 37] However, compared with the negatively charged MSNs that have a better endosomal escape ability, NCDs may need more time to escape from endosomes and lysosomes because of positive surface charge. In the present experiment, the positively charged NCDs enriched around the Cytoskeleton-Actin, possibly because the membrane potential is the major driving force which allows the entrance and accumulation of the cationic species into cell plasma. In addition, MCF-7 cells were also incubated with NCDs for 4 h and then imaged with CLSM (Figure S8). As expected, MCF-7 cells also showed multicolor emissions, further evidencing the potential of NCDs to serve as a good bioimaging agent for biolabeling.

3.4. Intracellular Imaging of Fe^{3+}

Besides, NCDs exhibited great promising in biological analysis. As Fe^{3+} commonly distributes in a variety of intercellular environment and plays ability to interact in biological reactions, it is extremely critical to establish a sensitive method for Fe^{3+} detection. Here we explored an effective approach to detect intracellular Fe^{3+} using NCDs as probe. The PL of the NCDs could be effectively quenched by Fe^{3+}. In this work, we propose Fe^{3+} ion could interact with phenolic hydroxyl groups and further coordinate with amino groups. Excited electrons could effectively transfer from the excited state to the half-filled 3D orbitals of Fe^{3+} ion, resulting in PL quenching. It is probably because of the nonradiative electron-hole annihilation. To investigate the mechanism of PL quenching of NCDs in the presence of

Fe^{3+}, fluorescence lifetime was conducted. As shown in Figure S9, for NCDs, the average lifetime of the fluorescence decay at 520 nm was 6.7 ns, which was longer than that of the treated with Fe^{3+} (2.8 ns). These results suggested that the dynamics quenching occurred between the surface of NCDs and Fe^{3+}. Figure 7a showed that the PL spectra of the NCDs after adding different concentration of Fe^{3+}. The PL intensity of NCDs at 623 nm decreased gradually with increasing concentrations of Fe^{3+}, indicating that the PL intensity of NCDs was effective Fe^{3+} concentration-dependent quenched. This quenching efficiency exhibited a linear detection range from 1 μM – 250 μM towards Fe^{3+}, with a low detection limit of 0.52 μM (calculated according to S/N=3) (Figure 7b).

Moreover, the complexity of intracellular environment makes great challenges for intercellular Fe^{3+} detection. Therefore, the relative selectivity experiments were realized. As shown in Figure 7c, the relative selectivity experiments, including many other metal ions and protein substrates, were realized and have shown that they had negligible influence on NCDs quenching, including Mn^{2+}, Co^{2+}, Ni^{2+}, Na^{+}, K^{+} and Mg^{2+}, suggesting this approach is feasible and reliable for Fe^{3+} detection. However, we found that Cu^{2+} may slightly influence the fluorescence emission of NCDs (Figure S10). In previous studies, functional amino groups could bind with Cu^{2+} ions to form cupric amine, resulting in quenching of fluorescence intensity of CDs through inner filter effect. Notably, Ag^{+} ions cannot inhibit the PL emission of CDs even it has similar reactivity with Cu^{2+}. It may result from there is no absorption in the PL emission spectra of NCDs for Ag-amine complexes, thus retain the PL emission of NCDs. We also found that Fe^{3+} exhibit greater binding affinity and chelating kinetics with NCDs than Cu^{2+}. As shown in Figure S10, with adding of Fe^{3+} of 50 μM, the fluorescence intensity of NCDs could be slightly quenched. With incubating of Cu^{2+}, the fluorescence intensity became further weaker. Here, we introduced triethanolamine (TEA) as chelating agent to circumvent quenching effect of Cu^{2+}. As shown in Figure S10, the mixture of Cu^{2+} and TEA has negligible influence on Fe^{3+} detection. All the results indicated that the NCDs could serve as probe to meet the selective and sensitive requirements for biological sensing. Consequently, NCDs were further demonstrated the availability for intracellular Fe^{3+} detection in MCF-7 cells. MCF-7 cells were pulsed with NCDs for 8 h, significant PL emission for the cytoplasm region could be clearly observed (Figure 7d and Figure S11). Pulsed a variety of concentrations of exogenous Fe^{3+}, this induced gradual PL intensity weaken, incorporating introducing of higher concentrations of exogenous Fe^{3+} into NCDs treated MCF-7 cells. The results indicated that the NCDs-based probe could be used for semi-quantitative detection of Fe^{3+} in cancer cells.

CONCLUSION

In summary, we presented a facile method to prepare bright and color-tunable NCDs from a specific kind of drug. Owing to the unique PL features and excellent biocompatibility, the as-prepared NCDs have great promise in cell imaging and sensitive detection of Fe^{3+} in living cells. Considering the huge number of drugs in the drug library, this approach can bring promising hints to develop a variety of high- quality drug derived NCDs for desired applications.

Supplementary Material

Refer to Web version on PubMed Central for supplementary material.

Acknowledgments

This work was partly supported by the National Institute of General Medical Sciences of the National Institutes of Health under Award Number R01GM122081. The content is solely the responsibility of the authors and does not necessarily represent the official views of the National Institutes of Health. D.D. would like to thank the National Natural Science Foundation of China (21575047) for partly supporting this work.

References

1. Resch-Genger U, Grabolle M, Cavaliere-Jaricot S, Nitschke R, Nann T. Quantum Dots versus Organic Dyes as Fluorescent Labels. Nat Meth. 2008; 5:763–775.
2. Gorris HH, Wolfbeis OS. Photon-Upconverting Nanoparticles for Optical Encoding and Multiplexing of Cells, Biomolecules, and Microspheres. Angew Chem Int Ed. 2013; 52:3584–3600.
3. Dou Q, Idris NM, Zhang Y. Sandwich-Structured Upconversion Nanoparticles with Tunable Color for Multiplexed Cell Labeling. Biomaterials. 2013; 34:1722–1731. [PubMed: 23201249]
4. Zhu L, Li X, Zhang Q, Ma X, Li M, Zhang H, Luo Z, Ågren H, Zhao Y. Unimolecular Photoconversion of Multicolor Luminescence on Hierarchical Self-Assemblies. J Am Chem Soc. 2013; 135:5175–5182. [PubMed: 23488680]
5. Fang Y, Guo S, Li D, Zhu C, Ren W, Dong S, Wang E. Easy Synthesis and Imaging Applications of Cross-Linked Green Fluorescent Hollow Carbon Nanoparticles. ACS Nano. 2012; 6:400–409. [PubMed: 22188541]
6. Kong B, Zhu A, Ding C, Zhao X, Li B, Tian Y. Carbon Dot-Based Inorganic–Organic Nanosystem for Two-Photon Imaging and Biosensing of pH Variation in Living Cells and Tissues. Adv Mater. 2012; 24:5844–5848. [PubMed: 22933395]
7. Li H, He X, Kang Z, Huang H, Liu Y, Liu J, Lian S, Tsang CHA, Yang X, Lee S-T. Water-Soluble Fluorescent Carbon Quantum Dots and Photocatalyst Design. Angew Chem Int Ed. 2010; 49:4430–4434.
8. Gupta V, Chaudhary N, Srivastava R, Sharma GD, Bhardwaj R, Chand S. Luminscent Graphene Quantum Dots for Organic Photovoltaic Devices. J Am Chem Soc. 2011; 133:9960–9963. [PubMed: 21650464]
9. Yan X, Cui X, Li L-s. Synthesis of Large, Stable Colloidal Graphene Quantum Dots with Tunable Size. J Am Chem Soc. 2010; 132:5944–5945. [PubMed: 20377260]
10. Baker SN, Baker GA. Luminescent Carbon Nanodots: Emergent Nanolights. Angew Chem Int Ed. 2010; 49:6726–6744.
11. Cao L, Meziani MJ, Sahu S, Sun Y-P. Photoluminescence Properties of Graphene versus Other Carbon Nanomaterials. Acc Chem Res. 2013; 46:171–180. [PubMed: 23092181]
12. Bao L, Liu C, Zhang Z-L, Pang D-W. Photoluminescence-Tunable Carbon Nanodots: Surface-State Energy-Gap Tuning. Adv Mater. 2015; 27:1663–1667. [PubMed: 25589141]
13. Nurunnabi M, Khatun Z, Huh KM, Park SY, Lee DY, Cho KJ, Lee Y-k. In Vivo Biodistribution and Toxicology of Carboxylated Graphene Quantum Dots. ACS Nano. 2013; 7:6858–6867. [PubMed: 23829293]
14. Li X, Liu Y, Song X, Wang H, Gu H, Zeng H. Intercrossed Carbon Nanorings with Pure Surface States as Low-Cost and Environment-Friendly Phosphors for White-Light-Emitting Diodes. Angew Chem Int Ed. 2015; 54:1759–1764.
15. Li W, Zhang Z, Kong B, Feng S, Wang J, Wang L, Yang J, Zhang F, Wu P, Zhao D. Simple and Green Synthesis of Nitrogen-Doped Photoluminescent Carbonaceous Nanospheres for Bioimaging. Angew Chem Int Ed. 2013; 52:8151–8155.
16. Jiang K, Sun S, Zhang L, Lu Y, Wu A, Cai C, Lin H. Red, Green, and Blue Luminescence by Carbon Dots: Full-Color Emission Tuning and Multicolor Cellular Imaging. Angew Chem Int Ed. 2015; 54:5360–5363.

17. Zhu A, Qu Q, Shao X, Kong B, Tian Y. Carbon-Dot-Based Dual-Emission Nanohybrid Produces a Ratiometric Fluorescent Sensor for In Vivo Imaging of Cellular Copper Ions. Angew Chem Int Ed. 2012; 51:7185–7189.
18. Yang S-T, Cao L, Luo PG, Lu F, Wang X, Wang H, Meziani MJ, Liu Y, Qi G, Sun Y-P. Carbon Dots for Optical Imaging in Vivo. J Am Chem Soc. 2009; 131:11308–11309. [PubMed: 19722643]
19. Li Y, Hu Y, Zhao Y, Shi G, Deng L, Hou Y, Qu L. An Electrochemical Avenue to Green-Luminescent Graphene Quantum Dots as Potential Electron-Acceptors for Photovoltaics. Adv Mater. 2011; 23:776–780. [PubMed: 21287641]
20. Tetsuka H, Asahi R, Nagoya A, Okamoto K, Tajima I, Ohta R, Okamoto A. Optically Tunable Amino-Functionalized Graphene Quantum Dots. Adv Mater. 2012; 24:5333–5338. [PubMed: 22833282]
21. Zhou J, Booker C, Li R, Zhou X, Sham T-K, Sun X, Ding Z. An Electrochemical Avenue to Blue Luminescent Nanocrystals from Multiwalled Carbon Nanotubes (MWCNTs). J Am Chem Soc. 2007; 129:744–745. [PubMed: 17243794]
22. Liu H, He Z, Jiang L-P, Zhu J-J. Microwave-Assisted Synthesis of Wavelength-Tunable Photoluminescent Carbon Nanodots and Their Potential Applications. ACS Appl Mater Interfaces. 2015; 7:4913–4920. [PubMed: 25671342]
23. Wang J, Wang C-F, Chen S. Amphiphilic Egg-Derived Carbon Dots: Rapid Plasma Fabrication, Pyrolysis Process, and Multicolor Printing Patterns. Angew Chem Int Ed. 2012; 51:9297–9301.
24. Qu S, Wang X, Lu Q, Liu X, Wang L. A Biocompatible Fluorescent Ink Based on Water-Soluble Luminescent Carbon Nanodots. Angew Chem Int Ed. 2012; 51:12215–12218.
25. Tang L, Ji R, Cao X, Lin J, Jiang H, Li X, Teng KS, Luk CM, Zeng S, Hao J, Lau SP. Deep Ultraviolet Photoluminescence of Water-Soluble Self-Passivated Graphene Quantum Dots. ACS Nano. 2012; 6:5102–5110. [PubMed: 22559247]
26. Wang W, Lu Y-C, Huang H, Feng J-J, Chen J-R, Wang A-J. Facile Synthesis of Water-Soluble and Biocompatible Fluorescent Nitrogen-Doped Carbon Dots for Cell Imaging. Analyst. 2014; 139:1692–1696. [PubMed: 24551871]
27. Peng J, Gao W, Gupta BK, Liu Z, Romero-Aburto R, Ge L, Song L, Alemany LB, Zhan X, Gao G, Vithayathil SA, Kaipparettu BA, Marti AA, Hayashi T, Zhu J-J, Ajayan PM. Graphene Quantum Dots Derived from Carbon Fibers. Nano Lett. 2012; 12:844–849. [PubMed: 22216895]
28. Liu R, Wu D, Liu S, Koynov K, Knoll W, Li Q. An Aqueous Route to Multicolor Photoluminescent Carbon Dots Using Silica Spheres as Carriers. Angew Chem Int Ed. 2009; 121:4668–4671.
29. Krysmann MJ, Kelarakis A, Dallas P, Giannelis EP. Formation Mechanism of Carbogenic Nanoparticles with Dual Photoluminescence Emission. J Am Chem Soc. 2012; 134:747–750. [PubMed: 22201260]
30. Pan L, Sun S, Zhang A, Jiang K, Zhang L, Dong C, Huang Q, Wu A, Lin H. Truly Fluorescent Excitation-Dependent Carbon Dots and Their Applications in Multicolor Cellular Imaging and Multidimensional Sensing. Adv Mater. 2015; 27:7782–7787. [PubMed: 26487302]
31. Wang L, Zhu S-J, Wang H-Y, Qu S-N, Zhang Y-L, Zhang J-H, Chen Q-D, Xu H-L, Han W, Yang B, Sun H-B. Common Origin of Green Luminescence in Carbon Nanodots and Graphene Quantum Dots. ACS Nano. 2014; 8:2541–2547. [PubMed: 24517361]
32. Ghosh S, Chizhik AM, Karedla N, Dekaliuk MO, Gregor I, Schuhmann H, Seibt M, Bodensiek K, Schaap IAT, Schulz O, Demchenko AP, Enderlein J, Chizhik AI. Photoluminescence of Carbon Nanodots: Dipole Emission Centers and Electron–Phonon Coupling. Nano Lett. 2014; 14:5656–5661. [PubMed: 25247753]
33. Shang J, Ma L, Li J, Ai W, Yu T, Gurzadyan GG. The Origin of Fluorescence from Graphene Oxide. Sci Rep. 2012; 2:792. [PubMed: 23145316]
34. Wang M, Liu H, Li L, Cheng YA. Fluorinated Dendrimer Achieves Excellent Gene Transfection Efficacy at Extremely Low Nitrogen to Phosphorus Ratios. Nat Commun. 2014(5):3035.
35. Yu C, Qian L, Ge J, Fu J, Yuan P, Yao SCL, Yao SQ. Cell-Penetrating Poly(disulfide) Assisted Intracellular Delivery of Mesoporous Silica Nanoparticles for Inhibition of miR-21 Function and Detection of Subsequent Therapeutic Effects. Angew Chem Int Ed. 2016; 55:9272–9276.

36. Feng T, Ai X, An G, Yang P, Zhao Y. Charge-Convertible Carbon Dots for Imaging-Guided Drug Delivery with Enhanced in Vivo Cancer Therapeutic Efficiency. ACS Nano. 2016; 10:4410–4420. [PubMed: 26997431]
37. Hu L, Sun Y, Li S, Wang X, Hu K, Wang L, Liang X-j, Wu Y. Multifunctional Carbon Dots with High Quantum Yield for Imaging and Gene Delivery. Carbon. 2014; 67:508–513.
38. Yu C, Li X, Zeng F, Zheng F, Wu S. Carbon-dot-based Ratiometric Fluorescent Sensor for Detecting Hydrogen Sulfide in Aqueous Media and Inside Live Cells. Chem Commun. 2013; 49:403–405.
39. Chen X, Jin Q, Wu L, Tung C, Tang X. Synthesis and Unique Photoluminescence Properties of Nitrogen-Rich Quantum Dots and Their Applications. Angew Chem Int Ed. 2014; 53:12542–12547.
40. Zhu S, Meng Q, Wang L, Zhang J, Song Y, Jin H, Zhang K, Sun H, Whang H, Yang B. Highly Photoluminescent Carbon Dots for Multicolor Patterning, Sensors, and Bioimaging. Angew Chem Int Ed. 2013; 52:3953–3957.
41. Zhou J, Yang Y, Zhang C. A Low-temperature Solid-phase Method to Synthesize Highly Fluorescent Carbon Nitride Dots with Tunable Emission. Chem Commun. 2013; 49:8605–8607.

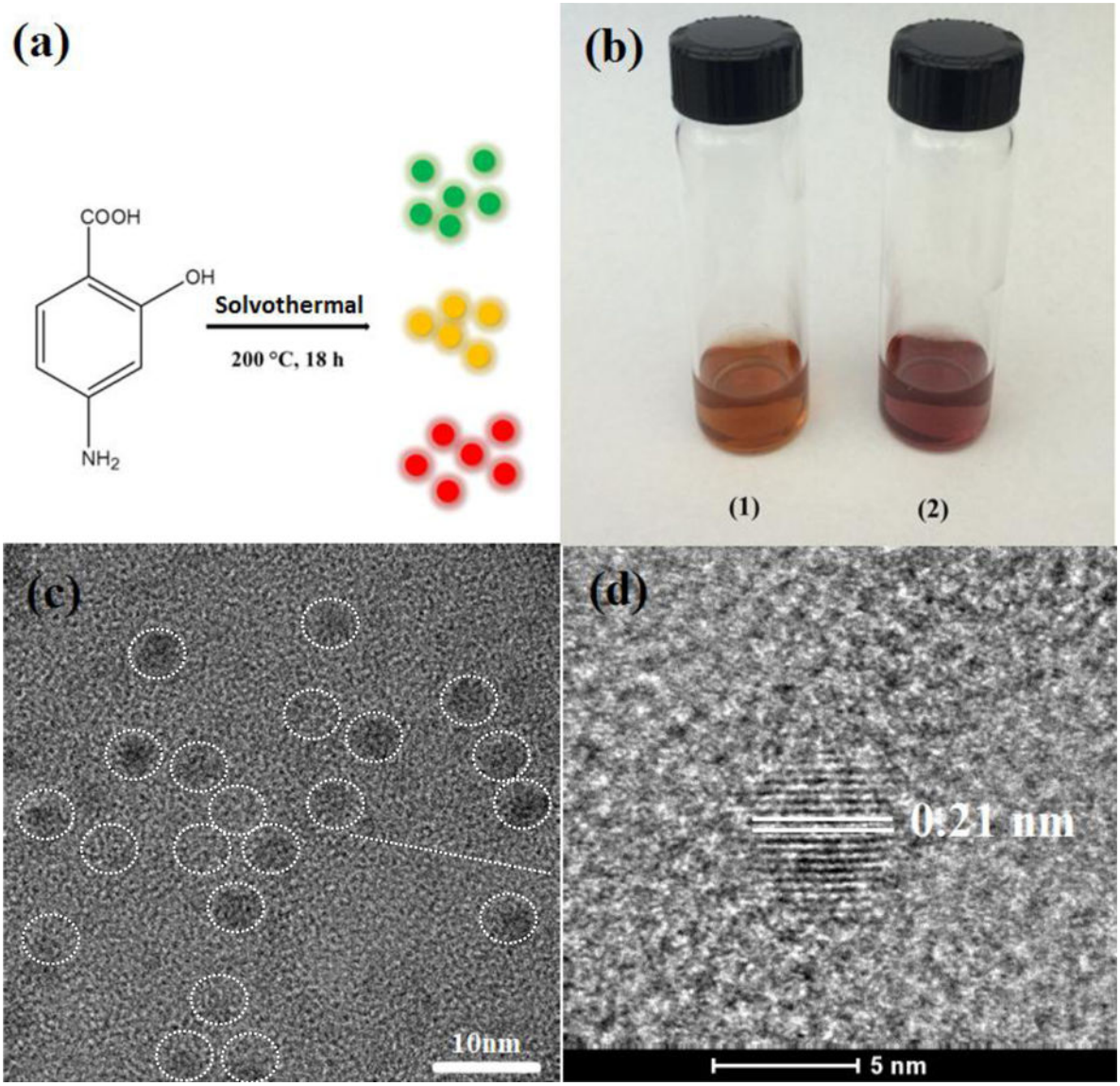

Figure 1.

(a) Preparation of the NCDs using ASA as precursor; (b) Photographs of NCDs dispersed in water (left) and PBS (right) with the concentration of 1 mg mL^{-1} in daylight; (c) TEM and (d) HRTEM image of NCDs.

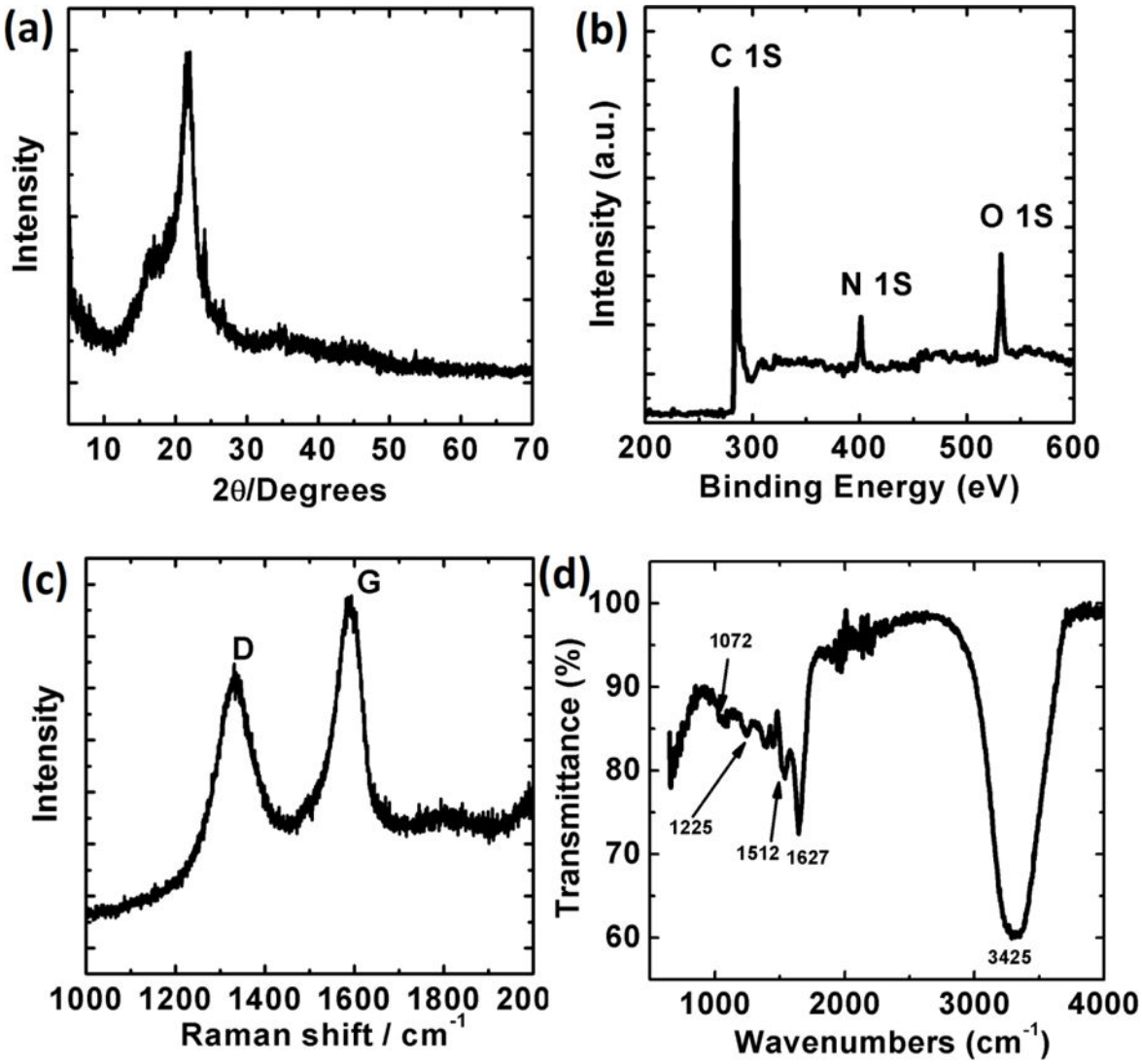

Figure 2.

(a) XRD; (b) XPS spectrum; (c) Raman spectrum and (d) FTIR spectra of NCDs. It contains the -OH, C=C, NH and C-OH groups.

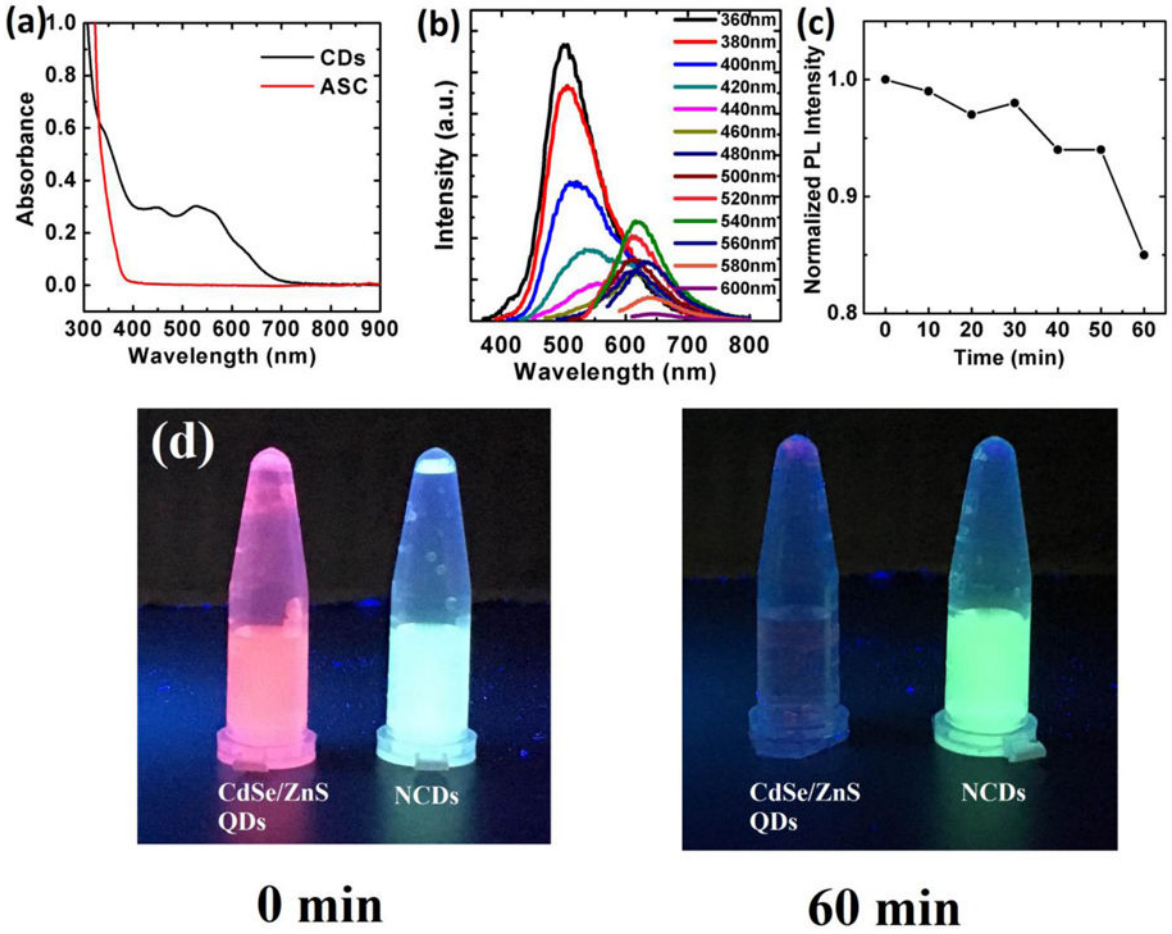

Figure 3.

(a) UV-Vis absorption spectra of NCDs (black line) and aminosalicylic acid (red line). (b) Fluorescent spectra of NCDs under different excitation wavelengths. (c) Excitation dependence of emission of NCDs in aqueous solution. (d) Photographs of CdSe/ZnS QDs and NCDs aqueous solution under UV irradiation for different times. All sample are continuously irradiated by a 500 W xenon lamp.

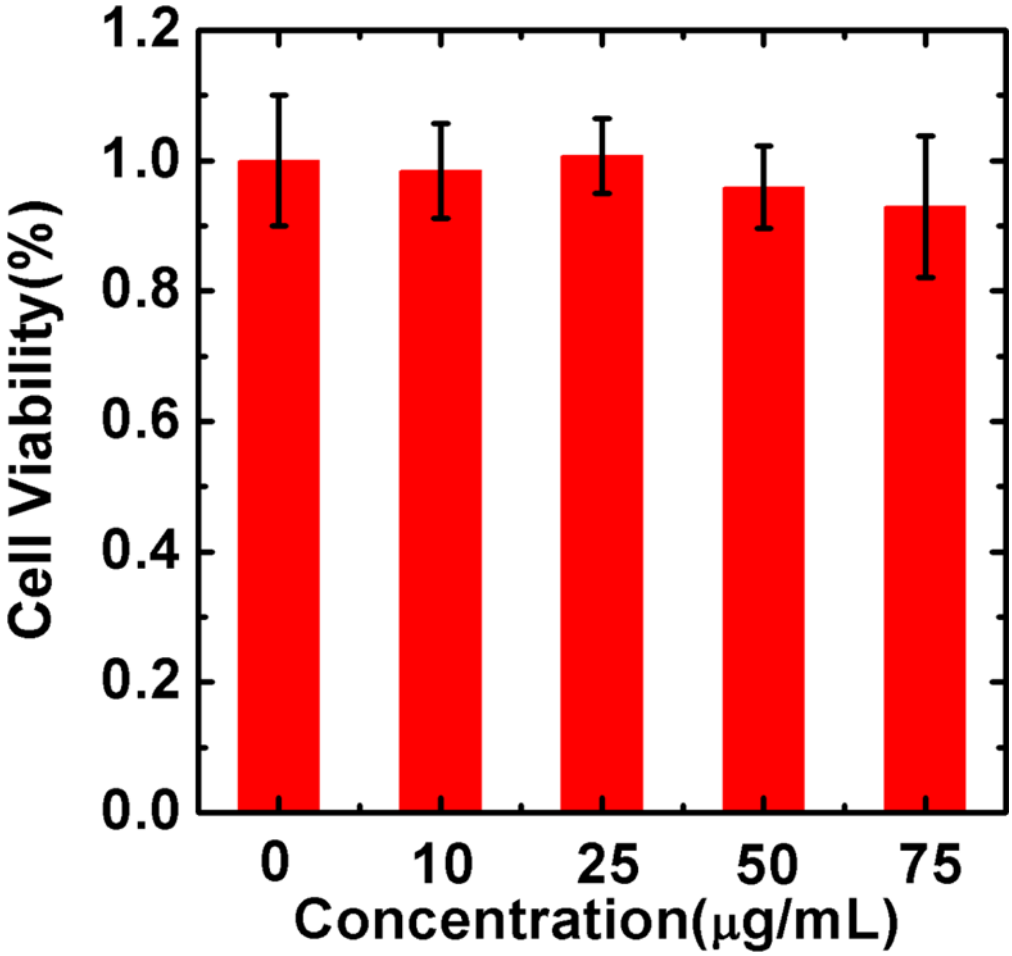

Figure 4.
Cellular cytotoxicity of the NCDs.

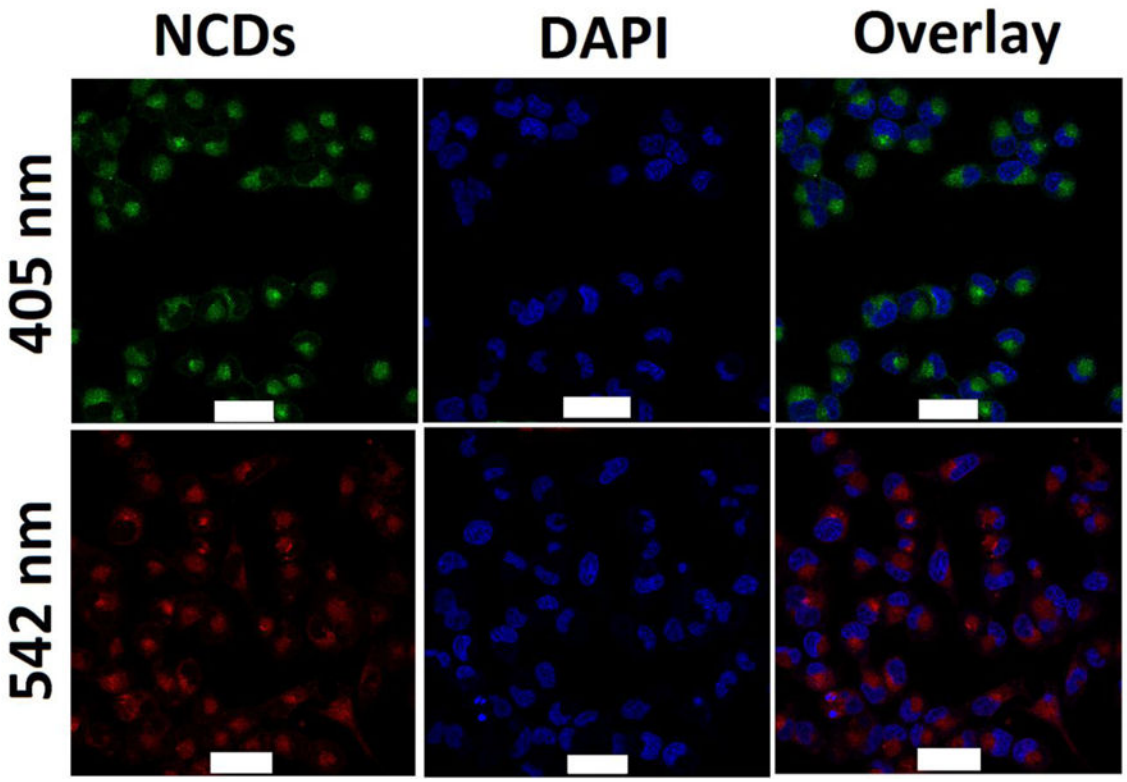

Figure 5.
CLSM fluorescence images of H1299 cells labeled with NCDs. Images were obtained with 405 nm and 542 nm laser. The scale bar is 50 μm.

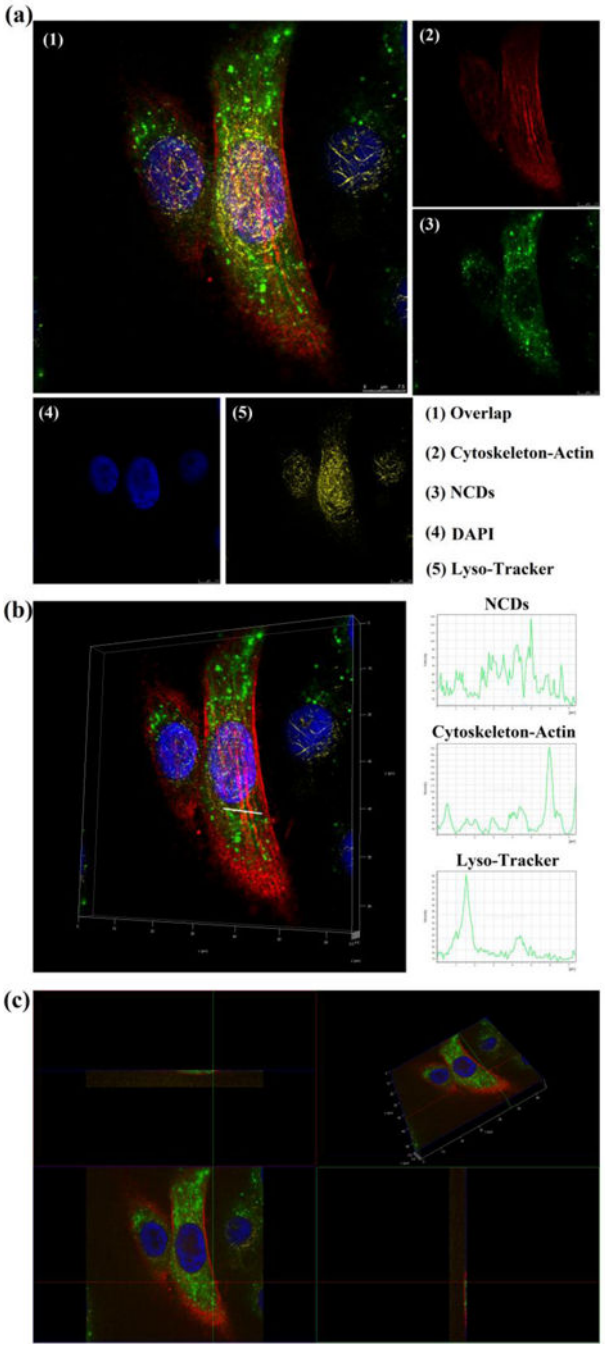

Figure 6.

(a) 3D projection showing Z-stack images of H1299 cells pulsed with NCDs (2 μg mL^{-1}) for 4 h, followed by staining with Cytoskeleton-Actin (red), Lyso-Tracker (yellow) and DAPI (Blue). CLSM images of overlay channel (1), Cytoskeleton-Actin (2), NCDs (3), DAPI stained nucleus (4) and Lyso-Tracker deep red stained lysosome (5). (b) Cellular uptake of NCDs under CLSM imaging. H1299 cells were incubated with NCDs for 4 h before measurement. 3D reconstructional CLSM images of the overlay channel of cellular NCDs (left); the quantification of fluorescent intensity of the line scanning profiles in the

corresponding CLSM images (right). (c) CLSM images of multiple cross-sections, exhibiting various locations of the NCDs within the cancer cells.

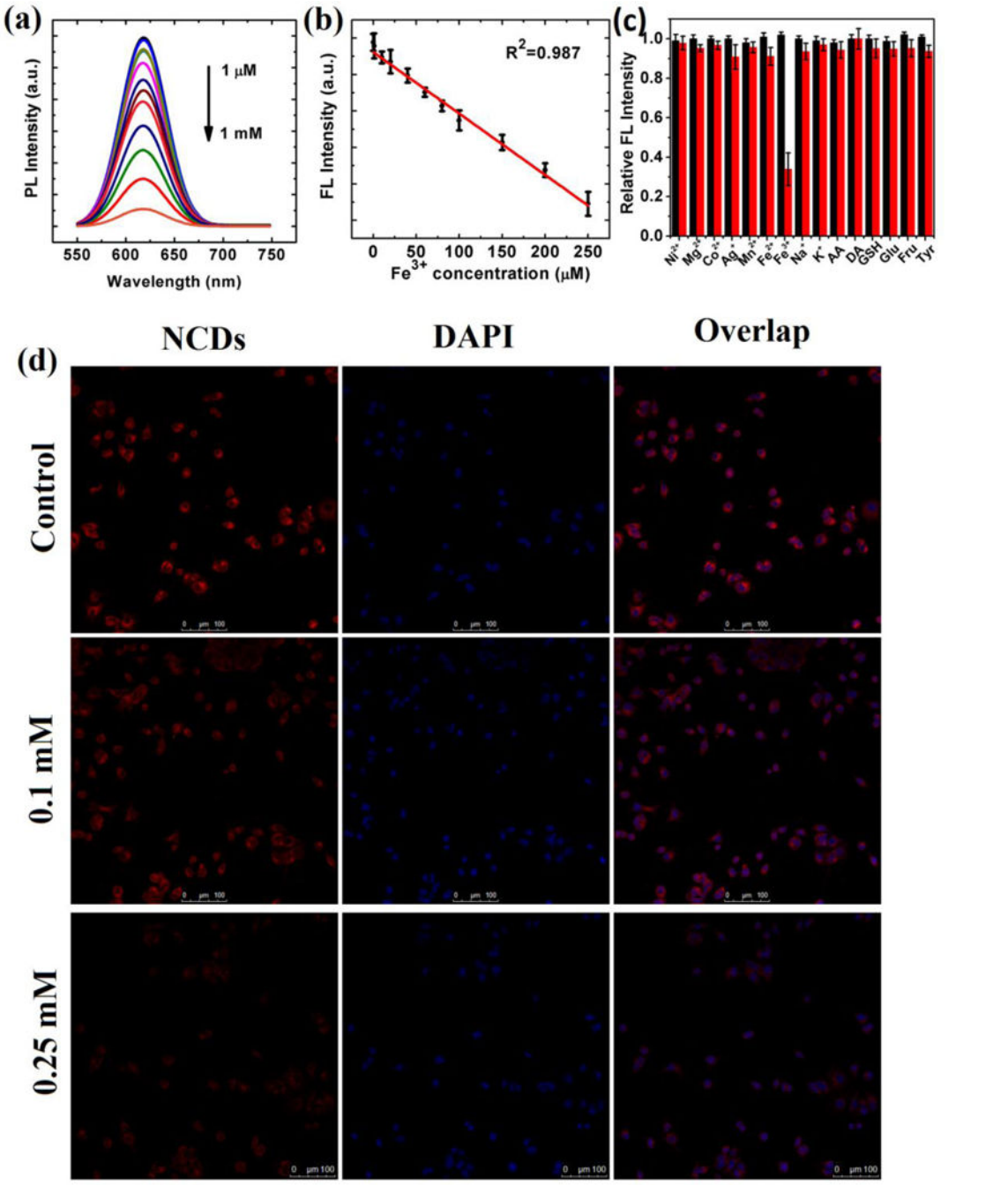

Figure 7.

(a) Fluorescence quenching in the presence of Fe^{3+} ion. The arrow exhibits the downward trend of fluoresence intensity as the concentration of Fe^{3+} increasing. (b) The calibration curve plotted on fluorescence intensity of NCDs treated with different concentrations of Fe^{3+}. (c) Comparison of fluorescence emission of NCDs after the addition of different metal ions. (d) CLSM fluorescence images of MCF-7 cells incubated with different concentration of NCDs/Fe^{3+} at 37 °C for 12 h. The top panels show the fluorescence images of MCF-7

cells without ion incubation. The central and bottom panels are cell images taken at ion concentration of 0.1 mM and 0.25 mM, respectively.